Effective potentials for dilute Bose-Einstein condensates

John L. Bohn,* B. D. Esry,† and Chris H. Greene
JILA and Department of Physics, University of Colorado, Boulder, Colorado 80309
(Received 10 December 1997)

We present a theoretical formulation of trapped, dilute Bose-Einstein condensates (BEC's) at zero temperature based on ordinary Schrödinger quantum mechanics. By a judicious choice of coordinates and of a variational trial wave function we reduce the many-atom problem to a *linear* Schrödinger equation that is easier to handle and interpret than the usual nonlinear Schrödinger equation of BEC theory. Ordinary quantum mechanics then reproduces, semiquantitatively, many of the main features of zero-temperature BEC, including the critical number of atoms in a condensate with negative scattering length. The procedure is similar in results, but completely different in spirit, to recent variational approaches to solving the nonlinear Schrödinger equation. Moreover, the present procedure represents a step in a systematic alternative method for computing quantitatively accurate wave functions for trapped bosonic atoms.
[S1050-2947(98)08107-4]

PACS number(s): 03.75.Fi, 31.15.Ja, 03.65.Ge

I. INTRODUCTION

Many-body quantum-mechanical systems continue to require new points of view to appreciate their behavior. Sometimes phenomena can be understood in terms of essentially independent-particle pictures, such as Rydberg electrons in atoms or elementary conduction in a simple metal, which is explained fairly well with a Drude model. On the other hand, some physical systems exhibit very strong correlations, such as the electrons and lattice ions in high-T_c superconductors. A full understanding of these materials still eludes physicists after a decade of effort [1].

In between these extremes lies another class of many-body systems, whose motion genuinely involves coordinated motion among the bodies, but which can be described by a few gross features. Thus in statistical mechanics the movements of 10^{23} atoms can be accurately summarized in terms of a few thermodynamic variables. Another example is afforded by the spectra of ''superdeformed'' nuclei; whatever many-body physics goes into producing these states, in the end their spectra are described simply in terms of highly elongated rotors [2]. This circumstance does not preclude the need for full many-body calculations of these spectra, but it does go a long way toward organizing the phenomena in our minds.

Another tractable many-body system that has emerged in recent years occurs in degenerate gases of alkali-metal atoms, cooled and magnetically trapped at sub-microKelvin temperatures. At the lowest temperatures, these gases undergo a phase transition and become Bose-Einstein condensates (BEC's) [3]. In the limit where the temperature vanishes, these gases no longer have a thermal component, and emerge as essentially a single lump of quantum stuff. In the resulting many-body system the individual bodies do not matter so much, since each atom lies within a deBroglie wavelength of its neighbors. In this case the individual atoms are not resolved, and we expect that the gas will be described, at least at some level, in terms of just a few degrees of freedom. A main goal of this paper is to reduce the condensate's description to motion in a *single* collective coordinate R, which represents roughly the extent of the condensate. Many condensate properties are described, at least qualitatively, by motion in the single coordinate R.

The diluteness of atomic BEC also assists in understanding it in simple terms. Being dilute, atomic BEC differs little from the gas that would be trapped if the atoms had no interaction at all, i.e., in an independent particle picture. The properties of BEC are thus amenable to treatment by perturbative methods. This situation stands in stark contrast to, say, superfluid helium, which is dense enough that perturbation theory proves inadequate.

The perturbation theory of choice these days for addressing atomic BEC is field theory. This approach begins with the independent-particle premise that individual atoms in definite single-particle orbitals of the trapping potential are free to interact. The appropriate set of orbitals is then determined self-consistently by accounting for the influence of atoms in one orbital on those in another. For atomic BEC a central theme that has emerged is the mean field theory, which produces the Gross-Pitaevskii (GP) equation, or nonlinear Schrödinger equation, [4]

$$i\hbar\frac{\partial\psi(\vec{r},t)}{\partial t}=-\frac{\hbar^2}{2m}\vec{\nabla}^2\psi(\vec{r},t)+V_{\rm trap}(\vec{r})\psi(\vec{r},t)+(N-1)\tilde{U}|\psi(\vec{r},t)|^2\psi(\vec{r},t). \quad (1.1)$$

Here m stands for the atomic mass, N the number of condensate atoms, and $V_{\rm trap}$ the potential due to the trapping field. The interatomic interactions are summarized in the final term on the right-hand side, where $\tilde{U}=4\pi\hbar^2a/m$ and a is the two-body s-wave scattering length between two atoms. The nonlinear term in Eq. (1.1) arises because a *representa-*

*Electronic address: bohn@murphy.colorado.edu
†Present address: ITAMP, Harvard University.

tive atom, with wave function ψ, feels the presence of the rest of the atoms according to their density, which is proportional to $(N-1)|\psi|^2$. Thus the mean field theory replaces a many-body wave function with a simpler function, the mean field ψ, which has now to be extracted from the nonlinear Eq. (1.1).

Equation (1.1), though nonlinear, has been solved by a number of groups [5–12]. These solutions, along with suitable generalizations, have quantitatively reproduced a number of observed condensate properties, such as ground-state shapes and energetics [13], excited state spectra [14], and coherence properties [15]. Field-theoretical methods are also making headway in understanding how these properties change at nonzero temperatures [16].

Further, Eq. (1.1) makes predictions concerning the instability of condensates whose atoms experience a net attractive interaction, as embodied in a negative s-wave scattering length a. An infinite, homogeneous condensate with attractive interactions proves unstable against collapse into a much denser, nonsuperfluid state [17]. However, Dodd *et al.* [7] have noted that a condensate confined to a finite region of space can exploit the kinetic energy of its confinement to stabilize itself, at least if the number of condensed atoms remains below some critical number N_c. A number of authors have predicted this critical number [6,7,18,19], and indeed, experiments at Rice University seem not to produce condensates containing larger numbers of atoms [20]. Such a condensate is regarded as metastable, however, and subject to decay by a sort of macroscopic tunneling of the condensate through an abstract potential barrier [21].

A second major goal of this paper is therefore to employ our one-coordinate reduction of the condensate as an alternative way to visualize what happens near this instability. Our model identifies a single coordinate R, essentially the mean condensate radius, as being most relevant to the gross features of the condensate. In what amounts to first-order perturbation theory, we average over all other coordinates of the full many-body wave function, yielding an effective potential $V_{\rm eff}(R)$ for the condensate's motion in R. A number of authors have also recently exploited the utility of an effective potential concept, with great success [8,18,21–24]. In all these cases, the authors solve Eq. (1.1) approximately by introducing a trial wave function (often a Gaussian) and mapping the variational energy as a function of its width. Our model chooses an alternative many-body trial wave function on different grounds, which nevertheless closely mimics the results of the other variational approximations, in particular by predicting the same critical number.

Our model takes a further step, however, inasmuch as the effective potential we derive really is an approximate potential in a real physical coordinate. We can therefore solve the resulting *linear* Schrödinger equation in R, whose results are in surprisingly good agreement with more accurate many-body approaches. Moreover, we arrive at our trial wave function from a systematic procedure that can be extended beyond the simple model presented here. The present model can then, in principle, be extended to a larger variational basis set, which should ultimately yield quantitative results. Our third goal is then to introduce this systematic method, as a basis for further work along this line.

II. FORMULATION

We consider a collection of N identical bosonic atoms of mass m confined magnetically in a trap approximated by a spherically symmetric harmonic oscillator potential with angular frequency ω. The traps currently used in experiments are not spherically symmetric, but this restriction does not affect our description of the qualitative features of the condensate. We will also assume throughout that the atom cloud is at zero temperature. Thus our approach will be that of ordinary Schrödinger quantum mechanics, in that we seek energy eigenstates of the N-boson system. The full N-body Hamiltonian of this system then reads

$$H=-\frac{\hbar^2}{2m}\sum_{i=1}^{N}\vec{\nabla}_i^2+\sum_{i=1}^{N}\frac{1}{2}m\omega^2 r_i^2+\sum_{i<j}U_{\rm int}(\vec{r}_i-\vec{r}_j), \tag{2.1}$$

where $U_{\rm int}$ stands for the pairwise atomic interaction potential. We feel free to ignore three-body and higher-order interaction potentials, again invoking the diluteness of the gas. We are in principle interested in solving the Schrödinger equation with this Hamiltonian,

$$H\psi(\vec{r}_1,\vec{r}_2,\ \ldots\ ,\vec{r}_N)=E\psi(\vec{r}_1,\vec{r}_2,\ \ldots\ ,\vec{r}_N). \tag{2.2}$$

Equation (2.2) represents a second-order partial differential equation in $3N$ coordinates, whose solution must moreover satisfy an elaborate set of boundary conditions incorporating the correct two-body wave function whenever any two atoms approach one another. It is an equation that can be ''solved fully'' in only a handful of experimental BEC laboratories around the world.

On the other hand, present-day experiments only probe the lowest several members of the spectrum of Eq. (2.2), and no experiment probes the condensate on the level of individual atoms. Indeed, to zeroth order the condensate is featureless and described only by its size. This motivates us to make a coordinate transformation, where one of the coordinates is the root-mean-squared radius of the atoms from the trap's center:

$$R\equiv\left(\frac{1}{\sum_i m_i}\sum_i m_i r_i^2\right)^{1/2}=\left(\frac{1}{N}\sum_i r_i^2\right)^{1/2}. \tag{2.3}$$

This kind of parametrization has a distinguished history in shell-model calculations of nuclei [25,26]. It has also played a fundamental role in understanding exotic multiply excited states of atoms [27], as well as reactive scattering in quantum chemistry [28,29]. For the purposes of the present article, we employ the associated methods in a rudimentary way, with the understanding that a more elaborate treatment is of course possible and ultimately desirable.

Mathematically R denotes the hyperradius of a $(3N-1)$-dimensional hypersphere in the $3N$-dimensional configuration space of the N atoms. Alternatively one can view R^2 as proportional to the trace of the moment of inertia tensor of the atom cloud. The remaining $3N-1$ atomic co-

ordinates are thus given in terms of the set of hyperangles, collectively denoted by Ω, that parametrize this hypersphere. Considerable freedom exists in choosing these angles, and several different conventions appear in the literature [30–33]. We will adopt the convention of Ref. [31], the relevant aspects of which we summarize in Appendix A.

Having made the transformation $(\vec{r}_1, \ldots, \vec{r}_N) \rightarrow (R, \Omega)$, we can likewise transform the Hamiltonian (2.1). Carrying out the transformation of the Laplacian, the kinetic energy becomes [32]

$$-\frac{\hbar^2}{2M}\left[\frac{1}{R^{3N-1}}\frac{\partial}{\partial R}\left(R^{3N-1}\frac{\partial}{\partial R}\right)-\frac{\mathbf{\Lambda}^2}{R^2}\right]. \tag{2.4}$$

In this expression $M = mN$ is the total mass of the atoms, and $\mathbf{\Lambda}$ stands for a ''grand angular momentum'' operator, defined analogously to a three-dimensional angular momentum [32],

$$\mathbf{\Lambda}^2 = -\sum_{i>j}\Lambda_{ij}^2, \quad \Lambda_{ij} = x_i\frac{\partial}{\partial x_j} - x_j\frac{\partial}{\partial x_i} \tag{2.5}$$

for all Cartesian components x_i of the $3N$-dimensional vector $(x_1, \ldots, x_N) \equiv (\vec{r}_1, \ldots, \vec{r}_{3N})$. Further, the oscillator potential transforms easily into

$$\sum_{i=1}^{N}\frac{1}{2}m\omega r_i^2 = \frac{1}{2}M\omega R^2. \tag{2.6}$$

To evaluate the interatomic interaction part of the Hamiltonian, we again exploit the diluteness of the condensate. Namely, we note that the atoms interact on scales less than ~ 10 nm, whereas the typical mean interatomic spacing is greater than ~ 100 nm. Thus as two atoms, let us say 1 and 2, approach each other, the dependence of the many-body wave function $\psi(\vec{r}_1, \vec{r}_2, \ldots, \vec{r}_N)$ will be essentially independent of coordinates $\vec{r}_3, \ldots, \vec{r}_N$. Moreover, its dependence on the difference $\vec{r}_1 - \vec{r}_2$ must reproduce the correct scattering wave function of the pair of atoms. But again, nothing is resolved on the 10-nm scale in a condensate, so all that really counts is the ''long-range'' behavior of this two-atom wave function, i.e., the scattering phase shifts. On scales larger than the 10 nm scattering region, we can recover the s-wave scattering phase shift from a contact potential of the form [34]

$$U_{\rm int}(\vec{r}_1 - \vec{r}_2) = \frac{4\pi\hbar^2 a}{m}\delta(\vec{r}_1 - \vec{r}_2); \tag{2.7}$$

we therefore adopt this form for $U_{\rm int}$ in Eq. (2.1). The simplicity of Eq. (2.7) conceals the fact that a three-dimensional delta-function potential is too singular to admit an analytical solution. In fact, Eq. (2.7) reproduces the scattering length only up to terms in the gradient of ψ. The subtleties involved in going beyond this approximation are treated in [35–37]. Nevertheless, for weakly interacting atoms we believe this approximation is justified. Note also the similarity of Eq. (2.7) to the interaction term of the nonlinear Schrödinger equation (1.1).

The transformed Schrödinger equation reads, after multiplying ψ by $R^{(3N-1)/2}$ to eliminate first derivatives in R,

$$\left\{-\frac{\hbar^2}{2M}\left[\frac{\partial^2}{\partial R^2} - \frac{(3N-1)(3N-3)}{4R^2} - \frac{\mathbf{\Lambda}^2}{R^2}\right] + \frac{1}{2}M\omega^2 R^2 + \sum_{i>j}\frac{4\pi\hbar^2 a}{m}\delta(\vec{r}_i - \vec{r}_j) - E\right\} R^{(3N-1)/2}\psi(R,\Omega) = 0. \tag{2.8}$$

So far the transformation has not bought us very much, since Eq. (2.8) is still a partial differential equation in $3N$ variables. We proceed from here by expanding the wave function into eigenfunctions of the $\mathbf{\Lambda}^2$ operator. These functions have been thoroughly studied in the literature [31–33], where they go by the name of ''hyperspherical harmonics.'' Their eigenvalue equation reads

$$\mathbf{\Lambda}^2 Y_{\lambda\mu}(\Omega) = \lambda(\lambda + 3N - 2)Y_{\lambda\mu}(\Omega), \tag{2.9}$$

where $\lambda = 0,1,2,\ldots$ denotes the order of the harmonic. The second index μ stands for the set of additional quantum numbers required to index the (generally very large) degeneracy of harmonics with the same value of λ. The harmonics $Y_{\lambda\mu}$ are multidimensional extensions of the familiar spherical harmonics; note that for a single particle $N = 1$, the eigenvalue in Eq. (2.9) reduces to the familiar $\lambda(\lambda+1)$ in three dimensions. The hyperspherical harmonics can be quite elaborate to evaluate and work with, but fortunately we do not need many of their detailed properties. We refer the interested reader to the literature for details [31–33].

Our construction of the approximate solution to Eq. (2.8) starts from an expansion of the wave function into the hyperspherical harmonics, which form a complete set on the surface of the hypersphere:

$$R^{(3N-1)/2}\psi(R,\Omega) = \sum_{\lambda\mu} F_{\lambda\mu}^{\lambda_0\mu_0}(R)Y_{\lambda\mu}(\Omega). \tag{2.10}$$

Here the indices $\lambda_0\mu_0$ label the linearly independent solutions to the Schrödinger equation; for notational simplicity, we will leave them out in what follows. This expansion reduces Eq. (2.8) to a set of coupled *ordinary* differential equations

$$\left\{ -\frac{\hbar^2}{2M}\left[\frac{d^2}{dR^2} - \frac{(3N-1)(3N-3)+4\lambda(\lambda+3N-2)}{4R^2}\right] + \frac{1}{2}M\omega^2R^2 \right\} F_{\lambda\mu}(R) + \sum_{\lambda'\mu'}\left[\sum_{i<j}\frac{4\pi\hbar^2 a}{m}\langle\lambda\mu|\,\delta(\vec{r}_i-\vec{r}_j)|\lambda'\mu'\rangle\right] F_{\lambda'\mu'}(R) = EF_{\lambda\mu}(R). \tag{2.11}$$

The radial functions in this system satisfy the small-R boundary conditions

$$F_{\lambda\mu} \to R^{\lambda_0+(3N-1)/2}\delta_{\lambda\lambda_0}\delta_{\mu\mu_0} \quad \text{as} \quad R\to 0, \tag{2.12}$$

reinforcing the fact that Eq. (2.8) is separable in hyperspherical coordinates at small R. The interaction term is now embodied in the matrix elements

$$\langle\lambda\mu|\,\delta(\vec{r}_i-\vec{r}_j)|\lambda'\mu'\rangle \equiv \int d\Omega\, Y^*_{\lambda\mu}(\Omega)\,\delta(\vec{r}_i-\vec{r}_j)\,Y_{\lambda'\mu'}(\Omega), \tag{2.13}$$

with the integral taken over the hypersphere of radius R. The integral (2.13) will generally depend on R.

If sufficiently many harmonics are included, Eqs. (2.11) can be used to extract the condensate spectrum from this linear system. Of course, a vast number of harmonics would be required to account in detail for the motion of every atom, but again, the gross features ought to emerge from a much smaller expansion. In particular, we will explore in this paper how well we can do by truncating the sum in Eq. (2.10) to a *single* term. In nuclear theory, this is known as the ''K-harmonic'' approximation [31]. We will use this term to distinguish the present treatment from more complete hyperspherical calculations to which we will sometimes refer. The natural choice for a single harmonic is Y_{00} (i.e., $\lambda=0$), which has no nodes in any of the hyperangular coordinates Ω. It therefore represents the longest-wavelength disturbance in all coordinates except R, and should best represent the smooth blob that is the condensate's ground state. (For those having little intuition about hyperspherical harmonics, it may be far from clear that this approximate wave function is sensible. We have tested it by plotting it alongside ground-state wave functions from the GP equation (1.1), and find that the two solutions are both nodeless in the hyperradius, and are remarkably similar at most hyperradii. Note also that this description becomes exact in the $R\to\infty$ limit, since the interaction dies off as $1/R^3$, faster than the kinetic energy $\propto 1/R^2$.)

We evaluate the interatomic interaction matrix element in Appendix B, arriving at the result

$$\sum_{i<j}\frac{4\pi\hbar^2 a}{m}\langle 00|\,\delta(\vec{r}_i-\vec{r}_j)|00\rangle = \sqrt{\frac{1}{2\pi}}\frac{\hbar^2 a}{m}\left[\frac{\Gamma(3N/2)}{\Gamma((3N-3)/2)N^{3/2}}\right]\frac{N(N-1)}{R^3}. \tag{2.14}$$

The expression in square brackets, depending on gamma functions, is nearly independent of N for $N>10$. Although we use its exact value in calculations, we will replace it in the formal expressions below by its asymptotic value $\xi\sim 1.837$. Note that Eq. (2.14) is qualitatively in accord with the mean field theory: each atom sees the rest with a mean energy $\sim(a/m)n$, with number density $n\sim(N-1)/R^3$. Since each of N atoms sees the same thing, the total energy of interaction scales as $\sim aN(N-1)/mR^3$, as in Eq. (2.14). This idea had already been articulated by Kagan *et al.* [10], and by Shuryak [18], who were among the first to quantify these notions.

Finally we arrive at the effective one-dimensional Schrödinger equation in the K-harmonic approximation for the condensate wave function:

$$\left[-\frac{\hbar^2}{2M}\frac{d^2}{dR^2} + V_{\rm eff}(R)\right]F(R) = EF(R), \tag{2.15a}$$

described by the effective potential

$$V_{\rm eff}(R) = \frac{\hbar^2}{2M}\frac{(3N-1)(3N-3)}{4R^2} + \frac{1}{2}M\omega^2R^2 + \xi\sqrt{\frac{1}{2\pi}}\frac{\hbar^2 a}{M}\frac{N^2(N-1)}{R^3}. \tag{2.15b}$$

We have cast Eqs. (2.15) in terms of the total mass $M=mN$, emphasizing that this equation approximates the quantum-mechanical motion of the condensate *as a whole*. Unsurprisingly, for $N=1$, Eq. (2.15) reduces to the equation for the radial motion of a single atom with zero angular momentum in a harmonic oscillator potential.

One essential feature of Eq. (2.15b) bears emphasizing. Even when all condensate atoms are presumed to have zero angular momentum about the trap's center, there remains an effective centrifugal barrier, represented by the term proportional to $1/R^2$ in Eq. (2.15b). This term summarizes concisely the kinetic energy cost of confining all atoms within a small region near the center of the trap, in accordance with the uncertainty principle. This energy is directly responsible for stabilizing an atomic condensate with $a<0$ against collapse.

We illustrate in Fig. 1 the general features of $V_{\rm eff}(R)$ versus R (in units of the harmonic oscillator length scale $\sqrt{\hbar/m\omega}$) for various values of the scattering length a. The heavy line shows $V_{\rm eff}$ for $a=0$, i.e., the noninteracting limit. In this case hyperradial solutions $\mathcal{R}_{\chi\lambda}(R)$ of Eq. (2.15) can be written analytically in terms of generalized Laguerre polynomials with χ radial nodes [31]. The quantum numbers χ, λ, and μ then completely characterize the eigenstates of N noninteracting atoms in a harmonic oscillator potential, with energy eigenvalues [31]

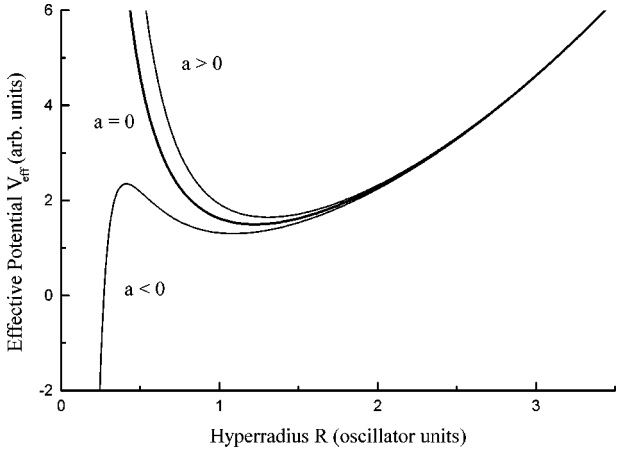

FIG. 1. Schematic of the effective potential, $V_{\text{eff}}(R)$, Eq. (2.15b). The heavy line represents the case where the scattering length $a=0$; its levels reproduce a subset of the harmonic oscillator levels, as detailed in Appendix C. For $a>0$ or $a<0$, V_{eff} becomes more repulsive or more attractive, as the upper and lower curves indicate.

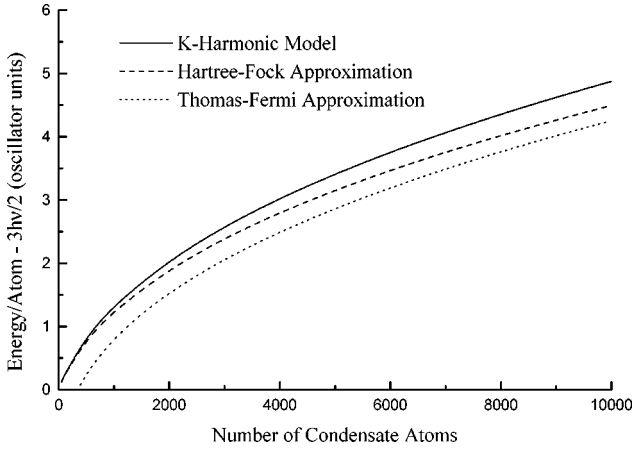

FIG. 2. Comparison of the K-harmonic, Hartree-Fock, and Thomas-Fermi estimates of the ground-state energy, for a condensate with $a=100$ bohr, and trap frequency $\nu=200$ Hz. The energy E_0 is plotted in the form $E_0/N-3h\nu/2$, to emphasize the contribution of the energy beyond that in the noninteracting case.

$$E_{\chi\lambda}=\hbar\omega\left(2\chi+\lambda+\frac{3N}{2}\right),\quad \chi=0,1,2,\ldots\ . \tag{2.16}$$

The associated eigenfunctions $\mathcal{R}_{\chi\lambda}(R)Y_{\lambda\mu}(\Omega)$ constitute a complete set, over all of configuration space, into which solutions of the interacting N-body problem can be expanded [38], although we will not do so in this paper. Appendix C details how the degeneracy of eigenstates with energy (2.16) equals the degeneracy expected from treating the problem in Cartesian coordinates.

For nonzero scattering length, V_{eff} acquires either a repulsive ($a>0$) or an attractive ($a<0$) interaction contribution, as indicated by the curves above and below the heavy curve, respectively. For $a<0$ the condensate is only metastable, living in the local minimum only until it tunnels through a potential barrier to the small-R region, where it accelerates inward to regions of configuration space with large radial kinetic energy. We will return to this metastability in some detail in Sec. IV. This basic physics of course also emerges in the variational approaches of [8,10,18,21–24]. Our own treatment is unique in assessing variationally the many-body Schrödinger equation (2.8) itself as opposed to the GP equation (1.1), resulting in a physical potential (2.15b) in a real coordinate R.

In a more complete calculation, there would be numerous additional potentials lying below V_{eff}, accounting for atom clouds in which atoms have recombined into molecules and clusters [43]. These curves are similar in shape to V_{eff}, but are shifted down by energies corresponding to the molecular binding energies, which are enormous on the scale of trap energies. Moreover, an accurate description of these potentials would entail hyperspherical harmonics with large numbers of nodes, to account for the close proximity of atoms in the molecules; accordingly, we ignore these potentials here. If calculated, these potentials would illustrate in more detail the fates of atoms lost to inelastic processes.

III. POSITIVE SCATTERING LENGTH CASE

For positive values of the scattering length a, the condensate energies deviate from those of the noninteracting condensate as the gas pushes harder against itself and against the walls of the trap. For definiteness we consider in this section a trap roughly approximating that in the JILA ^{87}Rb experiments, taking $a=100$ bohr, and a trap frequency $\nu=200$ Hz. For this case, we show in Fig. 2 the condensate's basic feature, namely, its ground-state energy. Here the energy E_0 for N atoms in the condensate is represented as $E_0/N-3h\nu/2$, to emphasize the deviation from the ideal gas result. The solid curve shows this quantity, versus the number of condensate atoms, according to the K-harmonic model. Below this curve lies the result of the Hartree-Fock (HF) approximation representing the solution to the nonlinear Schrödinger equation (1.1). The K-harmonic estimate lies mostly above that of the HF; since both are variational calculations, we conclude, not surprisingly, that the HF approximation is more accurate. Also plotted, as dotted lines, is an estimate arising from a Thomas-Fermi (TF) approximation, which solves Eq. (1.1) by ignoring kinetic energy altogether (e.g., Ref. [5]). For a modest number of atoms, the K-harmonic model is comparable with the TF approximation, although TF works better for large N, as it should. Considering the vast number of terms that have been neglected in the expansion (2.10), this agreement is already quite encouraging.

In fact, the K-harmonic approximation actually fares slightly better than the variational approach of, say, Stoof [21], and others like it. To see this, note that a Gaussian solution of the GP equation (1.1) implies a many-body trial wave function of the form $\exp(-r_1^2/q^2)\cdots\exp(-r_N^2/q^2)$, i.e., a Gaussian function of hyperradius, $\exp(-NR^2/q^2)$. Our trial wave function $F(R)$, by contrast, remains an *undetermined* function of hyperradius, and should thus be more flexible, arriving at a slightly better result. This turns out to be the case, although the K-harmonic energies are lower than the Gaussian variational energies by only about 1 part in 10^4.

Furthermore, we note in passing that some regimes even exist where the K-harmonic approximation is slightly *lower*

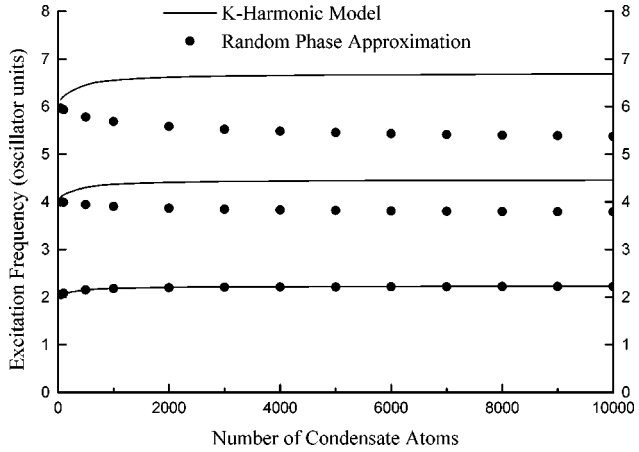

FIG. 3. Comparison of the K-harmonic and random-phase approximations to the low-lying excitation frequencies of the same condensate as in Fig. 2. This figure considers only excitations of spherical symmetry. The two approximations agree quite well for the first excitation, but disagree even on the trend with increasing N for higher excitations.

than the Hartree-Fock result, namely, for extremely tight traps and small numbers of atoms (e.g., fewer than about seven atoms). In this case, when the dimensionless parameter $(N-1)a/\sqrt{\hbar/m\omega}\approx 0.1$, the K-harmonic model slightly outperforms the Hartree-Fock model. This is, of course, not a physical regime yet, and so this result remains a curiousity.

The K-harmonic model can also approximate the excitation frequencies of the radial breathing modes, as illustrated in Fig. 3. The solid lines represent the K-harmonic results, while the points result from the random-phase approximation (RPA), which surpasses the HF approximation by incorporating some correlation between the HF orbitals [11]. The first excitation frequency agrees nearly perfectly between the two models, while the higher ones show significant discrepancies. The behavior of the K-harmonic model is easy to understand: Higher states in the spectrum, which extend to smaller values of R, feel more strongly the (positive) contribution from the $1/R^3$ interaction term, thus driving them higher relative to the ground state. In other words, for a breathing mode, the greater the excitation energy, the closer together the atoms will come *en masse*, increasing the effects of their interactions.

This simple interpretation, while applicable to the K-harmonic approximation, is obviously wrong in real life. Observed excitation frequencies invariably fall with increasing N in anisotropic traps [14]. Moreover, most other calculations (e.g., [11,39–42]) show *diminishing* excitation energies with increasing N. This circumstance points to a limitation of the K-harmonic model: while it gets something right about the radial energies, it is probably deficient in its ability to model the correct shape of excited-state wave functions. This deficiency will of course be ameliorated when more terms of the expansion (2.10) are incorporated.

The disagreement between the hyperspherical and RPA approaches is not limited to the relatively crude K-harmonic approximation employed here. In fact, for three atoms in a trap, a hyperspherical calculation can be performed with quantitative accuracy [43,44]. Viewed in the present context, such a treatment in effect takes all harmonics into account. This approach treats R as an adiabatic coordinate and solves Eq. (2.8) ''exactly'' after neglecting the hyperradial kinetic energy $\partial^2/\partial R^2$. This calculation produces a set of R-dependent potential curves analogous to, but containing more physics than, the single-harmonic approximation represented by Eq. (2.15b). Qualitatively, the spectrum of Fig. 3 persists: The adiabatic hyperspherical model predicts that all excitation frequencies *increase* from the noninteracting frequencies, while the RPA predicts that only the first excitation frequency is higher. It is unclear at present how much the ''exact'' adiabatic hyperspherical results will be altered by the addition of nonadiabatic effects, though their addition would provide a numerically exact solution with which to compare mean-field results. For now the lesson to be learned is that, even in the K-harmonic approximation, $V_{\rm eff}(R)$ apparently mimics the appropriate shape of the condensate's effective potential minimum reasonably well.

As a third test of the K-harmonic model's quantitative accuracy, we can also calculate the peak density of the condensate. As we will see in the next section, this density will have a bearing on the nature of the condensate's instability when $a<0$. To this end we recall the form of our many-body wave function,

$$\psi(\vec{r}_1,\ \ldots\ ,\vec{r}_N)=Y_{00}(\Omega)\frac{F(R)}{R^{(3N-1)/2}}, \tag{3.1}$$

where $F(R)$ is the solution of Eq. (2.15) that vanishes at $R=0$. The wave function ψ is normalized to unity over the entire $3N$-dimensional configuration space. To define a number density, we evaluate the ''density operator'' $\Sigma_i\delta(\vec{r}-\vec{r}_i)$ in the state (3.1):

$$\rho(\vec{r})\equiv\int d^3r_1\cdots d^3r_N|\psi(\vec{r}_1,\ \ldots\ ,\vec{r}_N)|^2\sum_i\ \delta(\vec{r}-\vec{r}_i), \tag{3.2}$$

which satisfies

$$\int\ d^3r\rho(\vec{r})=N. \tag{3.3}$$

The peak number density is then given by

$$\rho(0)=N\int_0^\infty dR|F(R)|^2\int\ d\Omega^{3N}|Y_{00}(\Omega)|^2\delta(\vec{r}_N), \tag{3.4}$$

where $\vec{r}_N$ is a representative atom coordinate and the sum over i is replaced by the prefactor N. The hyperangular integral in Eq. (3.4) is similar to that for the interaction term, and is evaluated in Appendix B. The result is

$$\rho(0)=N\frac{\xi}{\pi^{3/2}}\int_0^\infty dR\,\frac{|F(R)|^2}{R^3}. \tag{3.5}$$

Note in particular that the peak density is *not* proportional to $R^{(3N-1)}|F(R)|^2dR$ at $R=0$, which describes instead the probability that *all* atoms are found together in the center of the trap.

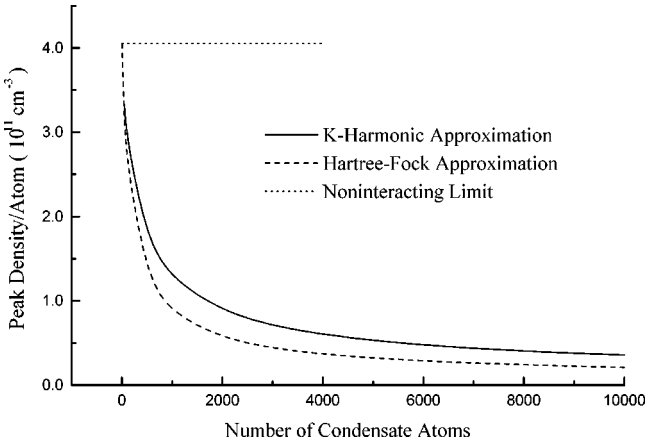

FIG. 4. Comparison of the K-harmonic and Hartree-Fock estimates of the peak density of the condensate considered in Figs. 2 and 3. The densities are normalized by the number of atoms, to emphasize the deviation from the noninteracting limit (shown as the dotted line).

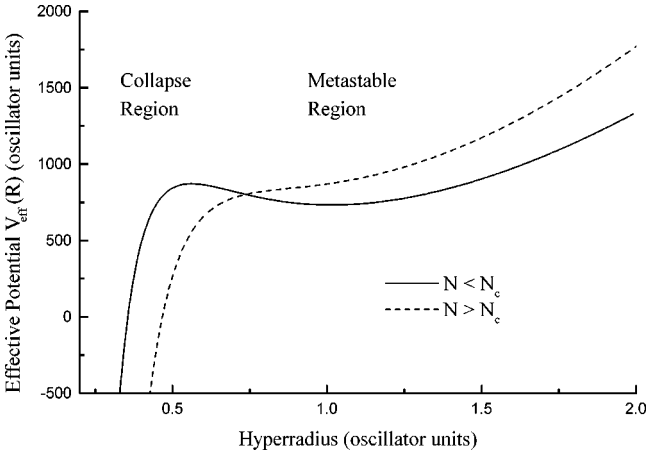

FIG. 5. Schematic of the effective potential $V_{\rm eff}$ for an attractive effective interaction, $a<0$. The solid curve represents a case where the number of atoms N is just less than the critical number N_c and a metastable condensate can exist in the potential's local minimum near $R=1$. This minimum therefore identifies the ''metastable'' region of R, separated by a potential barrier from the ''collapse region,'' where the atoms are strongly attracted to the trap's center by a $1/R^3$ attractive potential. The dashed line illustrates the case where $N>N_c$, and $V_{\rm eff}$ no longer possesses a local minimum. Compare to Fig. 2 of Ref. [22].

Figure 4 plots the peak number density in a condensate versus the number of condensate atoms, in both the K-harmonic and HF approximations. This density is normalized by the number of condensate atoms, to emphasize the difference from the noninteracting limit (which is a constant when plotted this way, as shown). The K-harmonic model thus accounts for most of the effect of interaction, even though its density overshoots the correct density be nearly a factor of two. The difference is a further indication of the inadequacy of the *ansatz* wave function $F(R)Y_{00}(\Omega)$ to describe the true wave function in detail. As we will see in the next section, the K-harmonic approximation fares much better for $a<0$ condensate wave functions.

IV. NEGATIVE SCATTERING LENGTH CASE

In this section we consider $a<0$, and choose trap parameters that approximate the conditions in the ^{7}Li experiments at Rice [20]. Namely, we set $a=-27.3$ bohr [45], and $\nu=(\nu_x\nu_y\nu_z)^{1/3}=144.6$ Hz, as has been done previously [19]. In real life, especially close to the critical number, the condensate is expected to be very nearly spherical [7]. We plot in Fig. 5 the general behavior of $V_{\rm eff}$ for N near the critical number N_c. When $N<N_c$ (solid line) $V_{\rm eff}$ possesses a local minimum that characterizes the ''metastable region,'' where a metastable condensate lives, stabilized by the $1/R^2$ effective centrifugal repulsion. At smaller R lies a potential barrier that separates the metastable region from the ''collapse region,'' which is dominated by the attractive $1/R^3$ component of $V_{\rm eff}$. As N grows, so does this component, until at $N\sim N_c$ the barrier vanishes altogether, as does the metastable region. For $N>N_c$ (dashed curve) $V_{\rm eff}$ is purely attractive, implying that the condensate cannot exist even metastably.

The argument of balancing kinetic and interaction energies to stabilize condensates is not new [10,18,21]. It has generally been approached by assessing these energies as they vary with the width of a variational trial function used to represent an orbital in the full condensate wave function. The width of this trial function, often of Gaussian form, represents in this case a variational parameter rather than a coordinate. Using such an analysis, Stoof identifies a potential energy functional [Eq. (21) of [21]] that enters into his field-theoretic treatment of metastable condensates. This functional has essentially the same form as our effective potential (2.15b). Other authors have followed suit, arriving at similar energy functionals [22–24]. In particular, Pérez-García *et al.* produce a figure essentially equivalent to Fig. 5. Shuryak plots a similar quantity, namely, an energy versus the central density of the condensate [18]. In all these cases the tunneling of the metastable condensate is viewed as an abstract process in a multidimensional field space of the possible condensate wave functions. The hyperspherical approach, by contrast, identifies a simple physical potential along a single adiabatic coordinate, and views the tunneling in the usual quantum-mechanical sense.

Once the condensate enters the collapse region, our simple model can no longer follow it. The real physics will involve enormous inward radial accelerations, increased atom collision rates, recombination into molecules and clusters, etc. Nevertheless, we can in our model describe the initial tunneling event that leads to this collapse. One major question regarding unstable condensates is, what is the nature of their demise? Dodd *et al.* [7] have argued that long before a macroscopic tunneling event swallows the condensate, two- and three-body losses will eject sufficiently many atoms to restabilize the cloud. Ueda and Leggett [24], following a lead from Kagan *et al.* [10], have recently argued that macroscopic tunneling can indeed be the faster process, when the number of atoms is very close to the critical number. In this section we will arrive at the same conclusion within the K-harmonic model.

A. Critical number

Our first task is to estimate the maximum number of identical bosons with negative scattering lengths that can be con-

densed. Within our model, we identify this critical number N_c as the number of atoms for which the barrier height in $V_{\rm eff}$ coincides with the minimum in the metastable region. (Strictly speaking, this approach will slightly overestimate the critical number, by ignoring the zero-point energy of the metastable state. It makes nevertheless a pretty good approximation.) To simplify the discussion, we write $V_{\rm eff}$ as

$$V_{\rm eff}(R)=\frac{A}{R^2}+BR^2+\frac{C}{R^3}, \tag{4.1}$$

with N-dependent coefficients that are apparent in Eq. (2.15b). The local maximum and local minimum of Eq. (4.1) coincide when the positive roots of $dV_{\rm eff}/dR$ coincide. Multiplying by R^4, we thus need to evaluate the positive roots of the fifth degree polynomial

$$R^4\frac{dV_{\rm eff}}{dR}=2BR^5-2AR-3C. \tag{4.2}$$

Analytic expressions for the roots of a fifth degree polynomial are cumbersome, if indeed they can be determined at all [46]. However, we need only the condition guaranteeing that the positive roots coincide, for which we can exploit a result of algebra known as Sturm's theorem [47], which provides an algorithm for counting polynomial roots. Sturm's theorem implies our condition is met when the coefficients of Eq. (4.2) satisfy

$$A^5=\frac{3^4\times 5^5}{2^{12}}C^4B. \tag{4.3}$$

Resubstituting the expressions for A, B, and C and assuming $N\gg 1$, we arrive at an expression for the critical number:

$$N_c\sim\frac{3\sqrt{3\pi}}{5^{(5/4)}\xi}\sqrt{\frac{\hbar}{m\omega}}\frac{1}{|a|}\sim 0.671\sqrt{\frac{\hbar}{m\omega}}\frac{1}{|a|}, \tag{4.4}$$

where ξ has been defined following Eq. (2.14). This expression has the usual dependence on the parameters m, ω, and a, and does reasonably well on the numerical prefactor. This value is 17% higher than the well-known value 0.573 obtained from numerical solutions of Eq. (1.1) (e.g., [7]). For the ^{7}Li trap parameters, the K-harmonic model predicts $N_c=1466$, in excellent agreement with variational estimates such as in [21,23]. This is not surprising, since these approaches and ours balance roughly the same kinetic and interaction energies.

Notice also that introducing additional hyperspherical harmonics, as in the expansion (2.10), will influence primarily the $1/R^3$ part of the interaction, where off-diagonal matrix elements will appear in Eq. (2.11). In such a case our effective potential will be obtained by treating R as an adiabatic coordinate, and diagonalizing Eq. (2.11) after setting $d^2F/dR^2=0$ in Eq. (2.11). This diagonalization will have the effect of further deepening the collapse region relative to the metastable region, thus diminishing N_c toward its correct value.

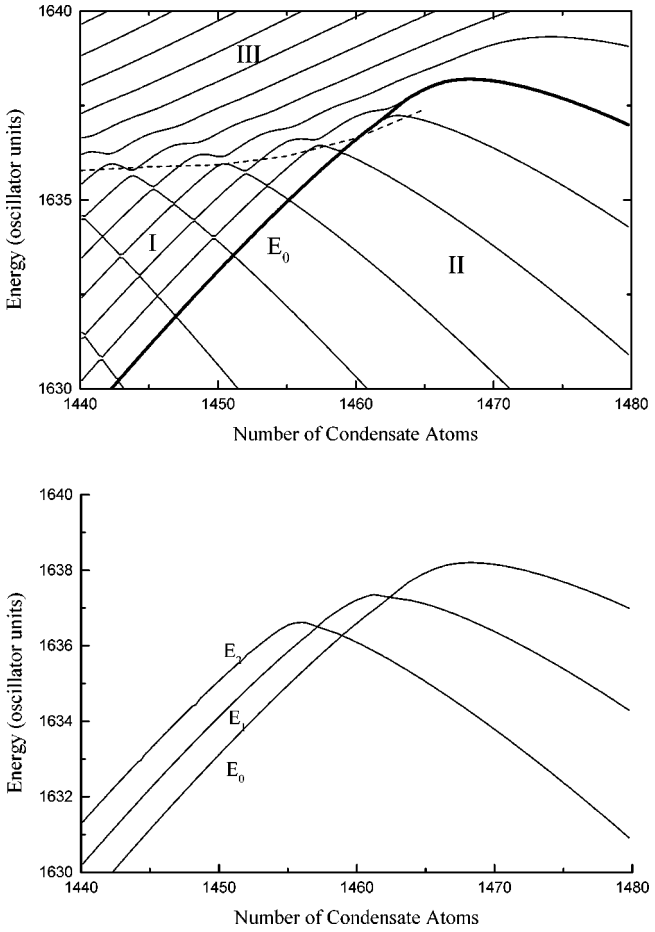

FIG. 6. A portion of the spectrum of energy levels vs N, within the K-harmonic approximation, for a condensate with $a=-27.3$ bohr and trap frequency $\nu=144.6$ Hz. In (a) the dashed line corresponds to the value of $V_{\rm eff}$ at the top of its potential barrier. Below this line, the levels denoted ''I'' correspond to wave functions localized in the metastable region of R depicted in Fig. 5. Their energies rise slowly as N grows. The levels denoted ''II'' correspond to wave functions localized in the collapse region of Fig. 5. Their energies drop steeply as N increases and the attractive $1/R^3$ part of $V_{\rm eff}$ deepens. The dashed line thus represents the transition between these types of localization. Above the dashed line are levels denoted ''III'' that lie above the barrier, and so sample both the metastable and collapsing regions. In (b), the lowest three metastable energy levels are extracted [the lowest, labeled E_0, is also indicated by the heavy line in (a)]. Each excited level drops in energy below the ground state as it tops the barrier and falls into the collapse region.

As $N\to N_c$ and the local maximum and local minimum of $V_{\rm eff}$ coincide, we note that the second derivative of $V_{\rm eff}$ will vanish at the point of coincidence. This means, in turn, that $V_{\rm eff}$ has no curvature and hence no oscillation frequency to lowest order. Here then is a classical explanation for the well-known ''softening'' of the condensate's modes for $a<0$.

B. Adiabatic energy level spectrum

We now address some additional details of the K-harmonic model. Figure 6(a) shows some of the energy levels in the potential $V_{\rm eff}$ versus N, which is taken as a

continuous parameter. Because of the $1/R^3$ singularity of $V_{\rm eff}$ at small R, we are obliged to impose artificial boundary conditions to avoid the infinitely many nodes of a wave function in this potential. We choose here and below to set the wave function $F(R)$ equal to zero at an inner cutoff point $R_{\rm cutoff}=0.6$ oscillator units. This limit lies well within the collapse region for the states of interest. The form of the wave function within the collapse region is of course unphysical, owing to the complications of small-R behavior neglected in the K-harmonic approximation.

Figure 6(a) shows three distinct types of behavior in the spectrum. In the lower left are levels (labeled ''I'') whose energies rise with increasing N; these represent the metastable levels, whose energies grow slightly sublinearly in N, owing to the net atomic attraction. In the lower half of the figure (below the dashed line) are a set of levels (labeled ''II'') whose energies decline with increasing N; these stand for the unphysical bound states trapped within the collapse region, and they get progressively deeper as this part of $V_{\rm eff}$ deepens. The dashed line in Fig. 6(a) represents the height of the barrier in $V_{\rm eff}$ as N varies. This curve marks roughly where each metastable level becomes unstable against spilling over the barrier. Above the dashed line lie levels (labeled ''III'') that therefore live only long enough to collapse.

The lowest-lying of the ''type I'' metastable levels is indicated by a heavy line in Fig. 6(a), where it is labeled E_0. This level stands for the metastable condensate's ''ground state.'' This curve is reproduced in Fig. 6(b), along with the energies E_1 and E_2 of the ''first two excited'' metastable states. When the number of atoms reaches the effective critical number 1460, the ground-state energy E_0 exceeds the barrier height, signaling the transition of this state from ''type I'' metastable to ''type II'' collapsing behavior; E_0 then turns down sharply. Note that the excited-state energies E_1 and E_2 make this transition for smaller numbers of atoms, since they are higher in energy to begin with.

Figure 7 further illustrates this transition by plotting the condensate's ground-state wave function $F(R)$ for various numbers of atoms. For $N=1450$ atoms, the barrier remains large, and the wave function is confined entirely to the metastable region. As the number of atoms rises, a portion of the wave function tunnels through the barrier, increasing the probability of a macroscopic tunneling event. For $N=1460$ atoms, the metastable state's energy is already at the top of the barrier [see Fig. 6(a)], and the wave function leaks readily into the collapse region. For even higher numbers, $N=1470$, the formerly metastable state lies entirely within the collapse region, and no condensate exists. In these figures the rapidly oscillating part of the wave function in the collapse region should be viewed as schematic, representing the rapid infall of the atom cloud.

We can extract from the spectrum the low-lying excitation frequencies of the metastable condensate, as plotted in Fig. 8(a). We again compare the K-harmonic results to those of the random-phase approximation. Both methods show the first excitation frequencies plummeting to zero (or below) as the number of atoms approaches the appropriate critical number. This reduction in excitation frequency represents the quantum-mechanical demonstration of mode softening for this system. Figure 8(b) replots the first excitation frequency versus the *scaled* number of atoms N/N_c. With this proviso, the agreement between K-harmonic and RPA models is again encouraging, as was the case for $a>0$. For the second excitation frequency, the agreement breaks down, just as before.

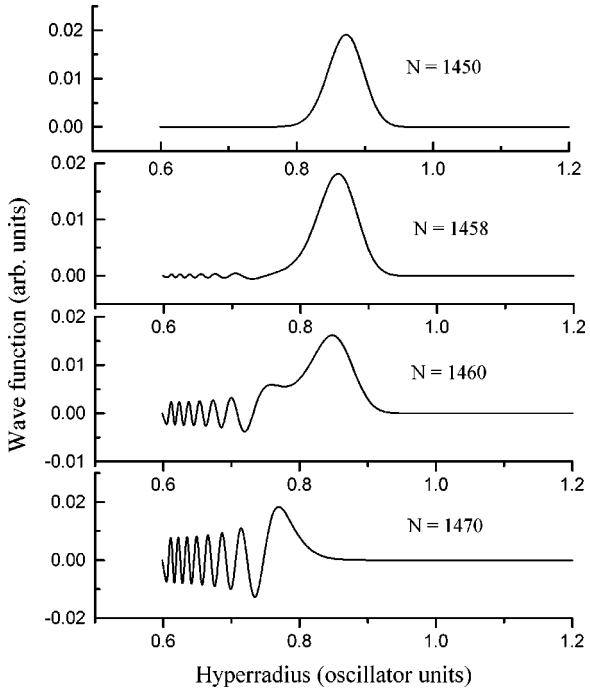

FIG. 7. Metastable condensate wave functions for the condensate labeled by energy E_0 in Fig. 6. As the number N of condensate atoms grows, the condensate's wave function is increasingly likely to tunnel through the barrier into the collapse region, until ultimately the entire condensate wave function is dominated by $V_{\rm eff}$'s attractive $1/R^3$ potential.

C. Decay rates

We can also extract the peak densities for metastable condensates from Eq. (3.4). This quantity is plotted in Fig. 9 and is compared to the Hartree-Fock result; both results are again scaled by their respective critical numbers. The adequacy of the K-harmonic model is much superior here to that in the $a>0$ case (cf. Fig. 4). This suggests that the hyperspherical harmonic Y_{00} captures much more accurately the shape of the true many-body wave function for the attractive case. The reason for this may be seen in the harmonic expansion (2.11): when larger values of λ are incorporated, they include a larger effective centrifugal barrier, $\propto\lambda^2/R^2$. These harmonics therefore have less to contribute to wave functions that occupy a smaller volume, i.e., which exist at smaller hyperradius R, which is the case for attractive condensates. We therefore anticipate that a full-blown hyperspherical treatment will have an easier time handling $a<0$ condensates than $a>0$ condensates.

From peak densities we can, in turn, estimate losses from the condensate due to two- and three-body processes. Following Dodd *et al.*, we identify a loss rate for an N-atom condensate [7]

$$\Gamma_N=\alpha N^2\int d^3r[\rho(\vec{r})]^2+LN^3\int d^3r[\rho(\vec{r})]^3. \quad (4.5)$$

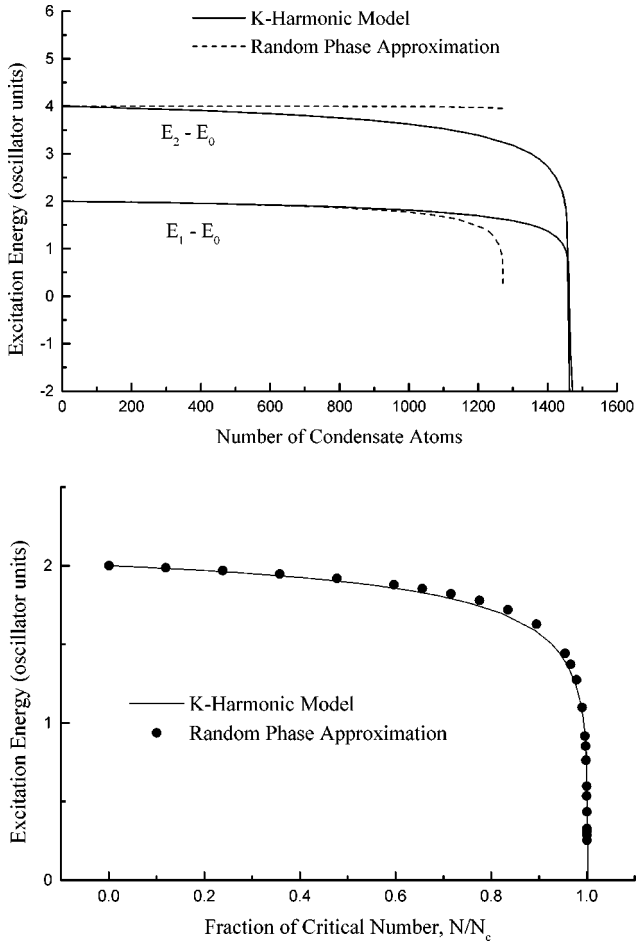

FIG. 8. Comparison of the K-harmonic and random-phase approximations to the first several excitation frequencies of the $a<0$ condensate considered in Fig. 6. In (a) the first excitation frequency in each model plummets to zero as the critical number of each model is approached. To remove the effect of different critical numbers in the two models, (b) plots the first excitation frequency vs the scaled number of atoms, N/N_c.

For ^{7}Li atoms trapped in their $|F=2,M=2\rangle$ states, the two-body loss rate, primarily due to dipolar relaxation, is $\alpha=1.2\times10^{-14}$ cm^3/sec [7] and the three-body recombination rate is estimated to be $L=2.6\times10^{-28}$ cm^6/sec [48]. We further approximate the total rate, in terms of the peak number densities, by

$$\Gamma_N\sim\{\alpha N^2[\rho(0)]^2+LN^3[\rho(0)]^3\}\frac{4}{3}\pi l^3, \tag{4.6}$$

whose last factor represents the condensate volume in a sphere of radius one oscillator unit, $l=\sqrt{\hbar/m\omega}$. This approximation gives loss rates of several hundred atoms per second near criticality, in rough agreement with the results of Dodd *et al.*, but necessarily overestimating Γ_N in the crude approximation (4.6).

As our final point, we use the K-harmonic model to estimate the rate of macroscopic tunneling, for comparison with the two- and three-body rates. To do this, we extract the WKB tunneling probability $\exp(-2\sigma)$ with

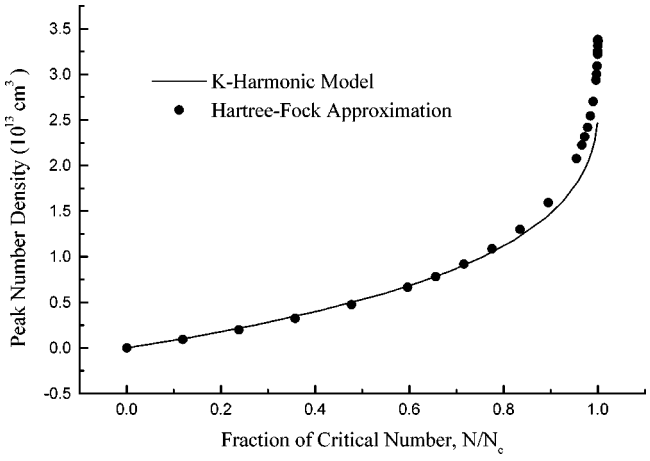

FIG. 9. Comparison of K-harmonic and Hartree-Fock approximation estimates of the peak condensate density for the condensate considered in Fig. 6. As in Fig. 8(b), N has been scaled by the appropriate critical number N_c. Both models show a sharp rise in density as the appropriate critical number is approached.

$$\sigma=\int_{R_{\rm in}}^{R_{\rm out}}dR\,\sqrt{\frac{2M}{\hbar^2}[V_{\rm eff}(R)-E]}. \tag{4.7}$$

This integral is taken between the inner ($R_{\rm in}$) and outer ($R_{\rm out}$) turning points of the barrier. E stands for the energy of the metastable condensate. Stoof has also cast condensate metastability in terms of a WKB-like integral [21], but he argues the point in a very formal way, in terms of an energy functional for condensates of Gaussian shape. Stoof's analysis has the advantage, however, that it can also estimate tunneling rates for condensates at nonzero temperatures. Ueda and Leggett similarly introduce a WKB integral without qualification, as if their variational width were a physical coordinate. In any event, the spirit is similar in all three approaches. To turn the probability (4.7) into a tunneling rate, we multiply by the frequency of the condensate's motion in the metastable part of the well, approximated by

$$\nu=\frac{1}{2\pi}\sqrt{\frac{1}{M}\frac{d^2V_{\rm eff}}{dR^2}(R_{\rm min})}, \tag{4.8}$$

where $R_{\rm min}$ denotes the position of $V_{\rm eff}$'s local minimum. Further, the macroscopic tunneling of the condensate takes *all* of the atoms with it. To obtain a tunneling rate in atoms/sec one then identifies a rate

$$\Gamma_N^{\rm tunnel}\sim N\nu\,\exp(-2\sigma). \tag{4.9}$$

Figure 10 plots the loss rates for the few-body and N-body processes for N near N_c. The tunneling rate has a strong exponential dependence on N, whereby its influence drops to insignificance if N is even five atoms below the critical number. Even accounting for order-of-magnitude uncertainties in the rates does not alter this basic conclusion. The tunneling rate is plotted only up to $N=1460$ atoms, beyond which even the metastable condensate's ground state lies higher in energy than the barrier. This circumstance identifies $N_c=1460$ atoms as the ''true'' critical number within our model.

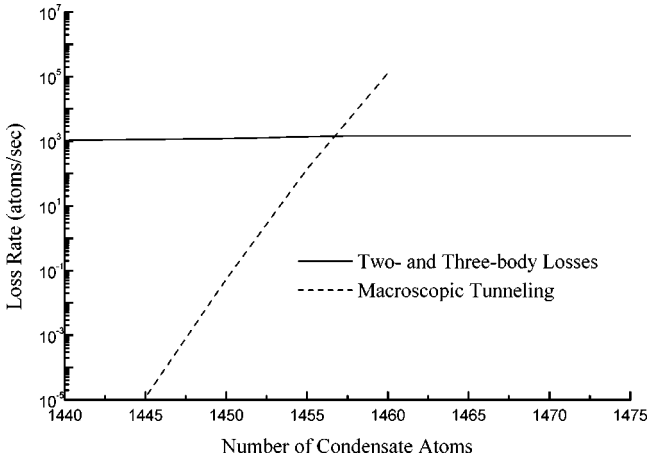

FIG. 10. The loss rate of atoms from the condensate due to two- and three-body processes (solid curve) and due to a macroscopic tunneling event (dashed line) for the condensate considered in Fig. 6. In this example the critical number is $N_c=1460$. Until the number of atoms reaches 1455 or so, the two- and three-body rates completely dominate the loss.

A linear fit of $\ln(\Gamma_N^{\text{tunnel}})$ versus N yields the dependence

$$\Gamma_N^{\text{tunnel}} \sim (2.7\times 10^5)\exp[\,1.6(N-N_c)\,] \text{ atoms/sec}, \tag{4.10}$$

assuming $N_c=1460$. The exponent 1.6 is about three times larger than Shuryak's estimate of 0.57, which was determined by projecting a Gaussian metastable wave function onto a variety of trial wave functions for the collapsed state [18]. Similarly, the WKB-like estimate of Stoof can be evaluated to yield an exponent ~ 0.65. If we artificially adjust the interaction term of V_{eff} to yield the correct critical number, we find that the exponent in the K-harmonic model drops to ~ 0.82, more in line with the other values. This is consistent with the fact that a more complete hyperspherical calculation will of course converge to the correct result. The more detailed analysis of Ueda and Leggett shows that the tunneling rate is actually not strictly exponential in N, but this distinction need not concern our qualitative discussion here.

Our main conclusion is then: if the condensate contains fewer than $\approx(N_c-5)$ atoms, it is likely to dribble away by two- and three-body losses rather than collapsing all at once in a macroscopic tunneling event. Even at high densities, it will be easier to bring pairs of atoms together than to bring the whole assembly of atoms together. The observation of macroscopic tunneling might just be possible, if the condition $N\sim N_c$ can be attained. This situation will probably be difficult to achieve by evaporative cooling, and will persist for a fraction of a second, making its observation a tricky challenge indeed. One possible solution would be to create a condensate very close to the critical number, then to tune the interaction strength so that N_c coincides with N. Such a tuning of scattering lengths may be possible using magnetic [49] or laser [50,51] fields. In addition, a technique was demonstrated recently for lowering to a temperature just above the transition temperature, then suddenly crossing the transition at will [52].

V. SUMMARY AND PROSPECTS

We have demonstrated an alternative approach to the physics of the ground state of a trapped many-boson system, from the point of view of ordinary Schrödinger quantum mechanics. We have selected a particularly useful variational trial wave function for the linear Schrödinger equation (2.8) that yields results similar to variational approaches to the nonlinear Schrödinger equation (1.1) in common use in BEC theory. This approximation produces surprisingly good quantitative results from a very simple model potential.

The present results are limited by our truncation to only a single term in the expansion (2.10). We anticipate that the results will improve as more of the expansion is included. If we appeal again to the basic simplicity in the shape of the condensate, we expect that the expansion need not contain too many terms before accurately representing a number of condensate properties. This approach also has the ability to describe condensates in nonspherical traps, provided that sufficiently many harmonics are included to represent the anisotropy of the condensate. These extensions of the K-harmonic model are presently being considered [53].

Finally, we remark that hyperspherical models are also suitable for describing mixtures of condensed atoms of different species. In this case each species i is accorded its own hyperradius R_i, and the overall hyperradius can be given as $(M_1+M_2)R^2=\Sigma_i M_i R_i^2$, with M_1 and M_2 the total masses of the two components. We expect this approach to shed light on the stability of double condensates [54,55], which possess three independent scattering lengths.

ACKNOWLEDGMENTS

The work of one of us (J.L.B.) was supported in part by the National Science Foundation and in part by the National Research Council. Two of us (B.E. and C.H.G.) acknowledge support from the Office of Basic Energy Sciences, U.S. Department of Energy.

APPENDIX A: HYPERSPHERICAL COORDINATES

The choice of a set of hyperspherical coordinates rests on first indentifying an appropriate set of Cartesian coordinates for the atoms, which can of course be done in many ways [31]. We will pick a particularly simple and convenient set of coordinates, namely, the radial vectors of each atom, $\vec{r}_1,\vec{r}_2,\ldots,\vec{r}_N$, with respect to the center of the trap. Then an obvious choice for $2N$ of the hyperangles is just the set of polar coordinates of the atoms,

$$\theta_1,\phi_1,\theta_2,\phi_2,\ldots,\theta_N,\phi_N. \tag{A1}$$

This leaves $N-1$ hyperangles to be chosen, which are conveniently defined as arctangents of ratios of radial distances. We will follow the convention of Ref. [31], defining these angles as follows:

$$r_N=\sqrt{N}R\,\cos\,\alpha_{N-1},$$

$$r_{N-1}=\sqrt{N}R\ \cos\ \alpha_{N-2}\sin\ \alpha_{N-1},$$

$$\ldots \tag{A2}$$

$$r_2=\sqrt{N}R\ \cos\ \alpha_1\sin\ \alpha_2\cdots\sin\ \alpha_{N-1},$$

$$r_1=\sqrt{N}R\ \sin\ \alpha_1\sin\ \alpha_2\cdots\sin\ \alpha_{N-1}.$$

In these expressions each angle α_j is restricted to run between 0 and $\pi/2$, to maintain positive definiteness of each r_i. This parametrization clearly satisfies our definition of hyperradius in Eq. (2.3). We remark in passing that these coordinates have also been used to parametrize the electronic coordinates in complex atoms [56].

Reference [31] also gives an explicit expression for the surface area element $d\Omega^{3N}$ of the hypersphere in $3N$ dimensions, which is conveniently parametrized in the present case as

$$d\Omega^{3N}=\prod_{i=1}^{N} d\phi_i d(\cos\ \theta_i)\prod_{j=1}^{N-1}\ \sin^{3j-1}\alpha_j\cos^2\ \alpha_j d\alpha_j. \tag{A3}$$

With this parametrization it is straightforward to evaluate the surface area of the hypersphere in terms of the gamma function,

$$\int\ d\Omega^{3N}=\frac{2\pi^{3N/2}}{\Gamma(3N/2)}. \tag{A4}$$

This integral implies in turn the normalization of the hyperspherical harmonic Y_{00}, which is a constant:

$$Y_{00}(\Omega)=\sqrt{\frac{\Gamma(3N/2)}{2\pi^{3N/2}}}. \tag{A5}$$

APPENDIX B: EVALUATION OF INTEGRALS

We wish to derive Eq. (2.14). To do this, we first note that by symmetry we need only evaluate the matrix element on the left for a single pair of atoms, whereby the left-hand side of Eq. (2.14) becomes

$$\sum_{i<j}\frac{4\pi\hbar^2 a}{m}\langle 00|\,\delta(\vec{r}_i-\vec{r}_j)|00\rangle = \frac{N(N-1)}{2}\frac{4\pi\hbar^2 a}{m}\langle 00|\,\delta(\vec{r}_1-\vec{r}_2)|00\rangle. \tag{B1}$$

We first rewrite the Dirac delta function in spherical coordinates,

$$\delta(\vec{r}_1-\vec{r}_2)=\frac{1}{r_1^2}\delta(r_1-r_2)\,\delta(\phi_1-\phi_2)\,\delta(\cos\ \theta_1-\cos\ \theta_2). \tag{B2}$$

Using Eq. (A3), the integration over the spatial angles is trivial:

$$\int\ d\phi_1 d(\cos\ \theta_1)\cdots\int d\phi_N d(\cos\ \theta_N)\,\delta(\phi_1-\phi_2)\times\delta(\cos\ \theta_1-\cos\ \theta_2)=(4\pi)^{N-1}. \tag{B3}$$

We next recast the radial part of the Dirac delta in terms of the α angles, using the definitions in Eq. (A2) and exploiting the fact that R is held constant:

$$\frac{1}{r_1^2}\delta(r_1-r_2)=\frac{1}{N^{3/2}R^3\sin^2\alpha_1\sin^3\alpha_2\cdots\sin^3\alpha_{N-1}}\times\delta(\sin\alpha_1-\cos\alpha_1). \tag{B4}$$

The integral over the volume element specified in Eq. (A3) and the delta function now factorizes into separate integrals for each α_j. For $j=2,\ldots,N-1$, the integrals are

$$\int_0^{\pi/2}\sin^{3j-1}\alpha_j\ \cos^2\alpha_j d\alpha_j\frac{1}{\sin^3\alpha_j}=\frac{1}{2}\frac{\Gamma((3j-3)/2)\Gamma(\frac{3}{2})}{\Gamma(3j/2)}, \tag{B5}$$

whereas the $j=1$ integral is

$$\int_0^{\pi/2}\sin^2\alpha_1\cos^2\alpha_1 d\alpha_1\frac{1}{\sin^2\alpha_1}\delta(\sin\ \alpha_1-\cos\ \alpha_1)=\frac{1}{2\sqrt{2}}. \tag{B6}$$

Multiplying the relevant factors together, and inserting the value (A5) for the hyperspherical harmonic, we arrive at the matrix element

$$\langle 00|\,\delta(\vec{r}_1-\vec{r}_2)|00\rangle=\frac{1}{2\sqrt{2\pi^3}}\frac{\Gamma(3N/2)}{\Gamma((3N-3)/2)}\frac{1}{N^{3/2}R^3}. \tag{B7}$$

Inserting this expression into Eq. (B1) finally produces the result (2.14).

We encounter a similar integral in Eq. (3.4). The only difference is in the factor $\delta(\vec{r}_1)$ instead of $\delta(\vec{r}_1-\vec{r}_2)$. The entire derivation goes through as above, except that the α_1 integration now reads

$$\int_0^{\pi/2}\sin^2\alpha_1\cos^2\alpha_1 d\alpha_1\frac{1}{\sin^2\alpha_1}\delta(\alpha_1)=1, \tag{B8}$$

leading to the result (3.5).

APPENDIX C: DEGENERACY OF OSCILLATOR STATES

In this Appendix we work out the degeneracy of N noninteracting atoms confined in a spherically symmetric harmonic oscillator potential. In the familiar Cartesian coordinates, if each degree of freedom i holds n_i quanta, then the total energy is

$$E_n=\hbar\omega\sum_{i=1}^{3N}\left(n_i+\frac{1}{2}\right)=\hbar\omega\left(n+\frac{3N}{2}\right),\quad n=\sum_i\ n_i. \tag{C1}$$

The degeneracy of levels with energy (C1) equals the number of ways in which n quanta can be distributed among $3N$ degrees of freedom, which is given by the binomial coefficient

$$\binom{n+(3N-1)}{n} = \frac{(n+(3N-1))!}{n!(3N-1)!}. \tag{C2}$$

In hyperspherical language, the energy eigenvalues are given by Eq. (2.16):

$$E_{\chi\lambda} = \hbar\omega\left(2\chi+\lambda+\frac{3N}{2}\right). \tag{C3}$$

For a given energy, we thus make the identification $2\chi+\lambda=n$. Avery gives an expression for the number of hyperspherical harmonics with a given value of λ ([32], p. 35):

$$\frac{(3N+2\lambda-2)(3N+\lambda-3)!}{\lambda!(3N-2)!} = \binom{\lambda+(3N-2)}{\lambda} + \binom{(\lambda-1)+(3N-2)}{(\lambda-1)}. \tag{C4}$$

To find the complete degeneracy, we must sum this expression for all allowed values of λ, consistent with $2\chi+\lambda=n$. Note that λ is restricted to values with the same parity as n, but the form of Eq. (C4) guarantees that all values of λ, even and odd, will appear in the sum. The total degeneracy is thus

$$\sum_{\lambda=0}^{n}\binom{\lambda+(3N-2)}{\lambda} = \binom{n+(3N-1)}{n}, \tag{C5}$$

in agreement with Eq. (C2). We have evaluated the sum (C5) using the following formal properties of binomial coefficients [57]:

$$\binom{-n}{k} = (-1)^k\binom{n+k-1}{k} \tag{C6}$$

and

$$\sum_{k=0}^{m}(-1)^k\binom{n}{k} = (-1)^m\binom{n-1}{m}. \tag{C7}$$

[1] J. G. Bednorz and K. A. Müller, Z. Phys. B **64**, 189 (1986); H. S. Takagi, S. Uchida, K. Kitazawa, and S. Tanaka, Jpn. J. Appl. Phys., Part 2 **26**, L123 (1987); E. Dagotto, Rev. Mod. Phys. **66**, 763 (1994).

[2] P. J. Twin *et al.*, Phys. Rev. Lett. **57**, 811 (1986); R. V. F. Janssens and T. L. Khoo, Annu. Rev. Nucl. Part. Sci. **41**, 321 (1991).

[3] M. H. Anderson, J. R. Ensher, M. R. Matthews, C. E. Wieman, and E. A. Cornell, Science **269**, 198 (1995); C. C. Bradley, C. A. Sackett, J. J. Tollett, and R. G. Hulet, Phys. Rev. Lett. **75**, 1687 (1995); K. B. Davis *et al.*, *ibid.* **75**, 3969 (1995).

[4] V. L. Ginzburg and L. P. Pitaevskii, Zh. Éksp. Teor. Fiz. **34**, 1240 (1958) [Sov. Phys. JETP **7**, 858 (1958)]; E. P. Gross, J. Math. Phys. **4**, 195 (1963).

[5] M. Edwards and K. Burnett, Phys. Rev. A **51**, 1382 (1995).

[6] P. A. Ruprecht, M. J. Holland, K. Burnett, and M. Edwards, Phys. Rev. A **51**, 4704 (1995).

[7] R. J. Dodd, M. Edwards, C. J. Williams, C. W. Clark, M. J. Holland, P. A. Ruprecht, and K. Burnett, Phys. Rev. A **54**, 661 (1996).

[8] G. Baym and C. J. Pethick, Phys. Rev. Lett. **76**, 6 (1996).

[9] F. Dalfovo and S. Stringari, Phys. Rev. A **53**, 2477 (1996).

[10] Yu. Kagan, G. V. Shlyapnikov, and J. T. M. Walraven, Phys. Rev. Lett. **76**, 2670 (1996).

[11] B. D. Esry, Phys. Rev. A **55**, 1147 (1997).

[12] M. Marinescu and A. F. Starace, Phys. Rev. A **56**, 570 (1997).

[13] M.-O. Mewes *et al.*, Phys. Rev. Lett. **77**, 416 (1996); M. Holland, D. S. Jin, M. L. Chiofalo, and J. Cooper, Phys. Rev. Lett. **78**, 3801 (1997).

[14] D. S. Jin, J. R. Ensher, M. R. Matthews, C. E. Wieman, and E. A. Cornell, Phys. Rev. Lett. **77**, 420 (1996); M.-O. Mewes *et al.*, *ibid.* **77**, 988 (1996).

[15] M. R. Andrews *et al.*, Science **275**, 637 (1997); A. Röhrl, M. Naraschewski, A. Schenzle, and H. Wallis, Phys. Rev. Lett. **78**, 4143 (1997).

[16] D. S. Jin, M. R. Matthews, J. R. Ensher, C. E. Wieman, and E. A. Cornell, Phys. Rev. Lett. **78**, 764 (1997); R. J. Dodd *et al.* (unpublished).

[17] P. Nozières and D. Pines, *The Theory of Quantum Liquids, Vol. II* (Addison-Wesley, Redwood City, CA 1990).

[18] E. V. Shuryak, Phys. Rev. A **54**, 3151 (1996).

[19] M. Houbiers and H. T. C. Stoof, Phys. Rev. A **54**, 5055 (1996).

[20] C. C. Bradley, C. A. Sackett, and R. G. Hulet, Phys. Rev. Lett. **78**, 985 (1997).

[21] H. T. C. Stoof, J. Stat. Phys. **87**, 1353 (1997).

[22] V. M. Pérez-García, H. Michinel, J. I. Cirac, M. Lewenstein, and P. Zoller, Phys. Rev. A **56**, 1424 (1997).

[23] A. L. Fetter, J. Low Temp. Phys. **106**, 643 (1997).

[24] M. Ueda and A. J. Leggett, Phys. Rev. Lett. **80**, 1576 (1998).

[25] L. M. Delves, Nucl. Phys. **9**, 391 (1959); **20**, 268 (1962).

[26] J. L. Ballot and M. Fabre de la Ripelle, Ann. Phys. (N.Y.) **127**, 62 (1980); M. V. Zhukov *et al.*, Phys. Rep. **231**, 151 (1993).

[27] J. H. Macek, J. Phys. B **1**, 831 (1968); U. Fano, Rep. Prog. Phys. **46**, 97 (1983); C. D. Lin, Phys. Rep. **257**, 1 (1995); J. L. Bohn, Phys. Rev. A **51**, 1110 (1995).

[28] F. T. Smith, J. Chem. Phys. **31**, 1352 (1959); Phys. Rev. **120**, 1058 (1960).

[29] V. Aquilanti, S. Cavalli, and G. Grossi, J. Chem. Phys. **85**, 1362 (1986); J. Lindberg *et al.*, *ibid.* **90**, 6254 (1989); R. T. Pack and G. A. Parker, *ibid.* **87**, 3888 (1987); J. M. Launay and M. LeDourneuf, Chem. Phys. Lett. **169**, 473 (1990).

[30] A. Erdélyi, W. Magnus, F. Oberhettinger, and F. G. Tricomi, *Higher Transcendental Functions* (McGraw-Hill, New York, 1953).

[31] Y. F. Smirnov and K. V. Shitikova, Fiz. Elem. Chastits. At. Yadra. **8**, 847 (1977) [Sov. J. Part. Nucl. **8**, 344 (1977)].
[32] J. Avery, *Hyperspherical Harmonics: Applications in Quantum Theory* (Kluwer, Dordrecht, 1989).
[33] U. Fano, D. Green, J. L. Bohn, and T. Heim (unpublished).
[34] N. F. Mott and H. S. W. Massey, *The Theory of Atomic Collisions*, 3rd ed. (Clarendon, Oxford, 1965), p. 777.
[35] A. Omont, J. Phys. (Paris) **38**, 1343 (1977).
[36] N. Y. Du and C. H. Greene, Phys. Rev. A **36**, 971 (1987); **36**, 5467(E) (1987).
[37] N. P. Proukakis, K. Burnett, and H. T. C. Stoof, Phys. Rev. A **57**, 1230 (1998), e-print cond-mat/9703199.
[38] M. Vallières, T. Das, and H. T. Coelho, Nucl. Phys. A **257**, 389 (1976).
[39] S. Stringari, Phys. Rev. Lett. **77**, 2360 (1996).
[40] M. Edwards, P. A. Ruprecht, K. Burnett, R. J. Dodd, and C. W. Clark, Phys. Rev. Lett. **77**, 1671 (1996).
[41] M. Fliesser, A. Csordás, P. Szépfalusy, and R. Graham, Phys. Rev. A **56**, R2533 (1997).
[42] P. Öhberg, E. L. Surkov, I. Tittonen, S. Stenholm, M. Wilkens, and G. V. Shlyapnikov, Phys. Rev. A **56**, R3346 (1997).
[43] B. D. Esry, C. H. Greene, Y. Zhou, and C. D. Lin, J. Phys. B **29**, L51 (1996).
[44] B. D. Esry and C. H. Greene (unpublished).
[45] E. R. I. Abraham, W. I. McAlexander, C. A. Sackett, and R. G. Hulet, Phys. Rev. Lett. **74**, 1315 (1995); E. R. I Abraham, N. W. M. Ritchie, W. I. McAlexander, and R. G. Hulet, J. Chem. Phys. **103**, 7773 (1995).
[46] D. Zwillinger, *CRC Standard Mathematical Tables and Formulae*, 30th ed. (Boca Raton, CRC Press, 1996), p. 83.
[47] *Handbook of Applicable Mathematics*, edited by W. Ledermann and S. Vasda (Wiley, New York, 1980), pp. 436–439.
[48] A. J. Moerdijk, H. M. J. M. Boesten, and B. J. Verhaar, Phys. Rev. A **53**, 916 (1996).
[49] E. Tiesinga, B. J. Verhaar, and H. T. C. Stoof, Phys. Rev. A **47**, 4114 (1993).
[50] P. O. Fedichev, Yu. Kagan, G. V. Shlyapnikov, and J. T. M. Walraven, Phys. Rev. Lett. **77**, 2913 (1996).
[51] J. L. Bohn and P. S. Julienne, Phys. Rev. A **56**, 1486 (1997).
[52] H.-J. Miesner, D. M. Stamper-Kurn, M. R. Andrews, D. S. Durfee, S. Inouye, and W. Ketterle, Science **279**, 1005 (1998).
[53] A. Hooker (unpublished).
[54] B. D. Esry, C. H. Greene, J. P. Burke, Jr., and J. L. Bohn, Phys. Rev. Lett. **78**, 3594 (1997).
[55] C. K. Law, H. Pu, N. P. Bigelow, and J. H. Eberly, Phys. Rev. Lett. **79**, 3105 (1997); H. Pu and N. P. Bigelow, *ibid.* **80**, 1130 (1998); **80**, 1134 (1998).
[56] M. Cavagnero, Phys. Rev. A **30**, 1169 (1984); **33**, 2877 (1986); **36**, 523 (1987).
[57] A. Jeffrey, *Handbook of Mathematical Formulas and Integrals* (Academic, San Diego, 1995), p. 31.